Human Hair Graying is Naturally Reversible and Linked to Stress

Ayelet Rosenberg[1], Shannon Rausser[1], Junting Ren[2], Eugene Mosharov[3, 4],
Gabriel Sturm[1], R Todd Ogden[2], Purvi Patel[5], Rajesh Kumar Soni[5], Clay Lacefield[4],
Ralf Paus[6], Martin Picard[1, 4, 7,]*

[1] Department of Psychiatry, Division of Behavioral Medicine, Columbia University Medical Center, New York, NY, USA

[2] Department of Biostatistics, Mailman School of Public Health, Columbia University Medical Center, New York, NY, USA

[3] Department of Psychiatry, Division of Molecular Therapeutics, Columbia University Medical Center, New York, NY, USA

[4] New York State Psychiatric Institute, New York, NY USA

[5] Proteomics and Macromolecular Crystallography Shared Resource, Columbia University Irving Medical Center, New York, NY, USA

[6] Dr. Phillip Frost Department of Dermatology & Cutaneous Surgery, University of Miami Miller School of Medicine, Miami, FL, USA & Centre for Dermatology Research, University of Manchester, Manchester, UK

[7] Department of Neurology, H. Houston Merritt Center, Columbia Translational Neuroscience Initiative, Columbia University Medical Center, New York, NY, USA

Summary

Hair graying is a universal hallmark of aging[1] but its mechanisms are insufficiently understood[2] and its reversibility in humans remains uncertain. Moreover, while psychological stress accelerates human biological aging[3,4] and triggers hair graying in animals[5], no prior study has longitudinally examined the stress-to-hair graying connection in humans. Here we develop an approach to quantitatively profile natural graying events and their associated proteomic signatures along individual human hairs, resulting in a quantifiable physical timescale of aging. Using this approach, we identify white hairs that naturally regain pigmentation within days to weeks in healthy young individuals across sex, ethnicities, ages, and body regions, demonstrating that human hair graying is naturally reversible. Proteomic analysis of matched dark and white hairs replicated across two independent experiments show that graying is marked by the upregulation of proteins related to energy metabolism, mitochondria, and antioxidant defenses. Coordinated graying and reversal also occur simultaneously across multiple scalp hair follicles of a person, suggesting that unknown systemic factors influence hair graying patterns. Combining hair pigmentation profiling and proteomics at the single hair shaft level, we also report hair graying and reversal occurring in parallel with behavioral and psychological stressors. A computational simulation of life-long and stress-induced hair graying suggests a threshold-based mechanism for the rapid reversibility of graying. Together, these findings document the reversibility of hair graying in humans and provide a new model to examine the modifiability of human aging.

Keywords: human aging; hair graying; reversal; psychological stress; mitochondria.

Hair graying is a ubiquitous, visible, and early feature of human aging. The onset of hair graying varies between individuals based on genetic and other biobehavioral factors, but most people experience depigmentation of a progressively large number of hair shafts (HS) from their third decade onward, known as achromotrichia or canities[6]. The color in pigmented HS is provided by melanin-loaded melanosomes continuously supplied to the trichocytes of the growing hair shaft by melanocytes of the hair follicle pigmentary unit (HFPU)[1]. Aging-related graying involves melanocyte stem cell (MSC) exhaustion[7], neuroendocrine alterations[2], and other factors, with oxidative damage to the HFPU likely being the dominant, initial driver[2,8,9].

Although isolated cases of drug- and mineral deficiency-induced depigmentation or repigmentation have been reported[10-14], reflecting the influence of environmental inputs into HFPU function[15], hair graying is generally considered a progressive and irreversible age-related process. Likewise, whether psychological stress influences hair graying has been examined in mice[5] but remains uncertain and insufficiently documented in humans[9]. The paucity of data in humans is mostly due to the lack of sensitive methods to precisely correlate stressful psychobiological processes with hair pigmentation and graying events at the single-follicle level.

Results

Mapping hair pigmentation patterns (HPPs)

To overcome this limitation and to explore hair graying as a quantifiable, personalized live bioarchive of human aging, we developed an approach to digitize hair pigmentation patterns (HPPs) at high resolution across the length of single human HS. Combined with the known hair growth rate (~1.0-1.3cm per month[16]), this approach provides the necessary spatio-temporal resolution to map individualized HPPs and graying transitions along single hairs and link them to specific moments in time with unprecedented accuracy. Using this methodology, similar to dendrochronology where tree rings represent elapsed years[17], hair length reflects time and the HS is viewed as a physical time scale whose region proximal to the scalp has been most recently produced by the HF, and where the hair tip represents weeks to months in the past, depending on the HS length.

To examine HPPs in human hairs, we plucked, imaged, digitized, and analyzed hairs (n=397) from 14 healthy donors (**Figure 1A**) (see Methods for details). Three main pigmentation patterns initially emerged from this analysis: i) Hairs with constant high optical density (*Dark*), ii) Hairs with constant low optical density (*White*); iii) Initially dark hairs that undergo complete graying over the course of a single hair follicle growth cycle (*Transition*) (**Figure 1B-C**). Dark-to-white transitions demonstrate the existence of rapid depigmentation events within a single

3

growth phase (anagen) of the hair cycle[18,19]. We confirmed that compared to dark hairs still harbouring their "young" pigmentary state, the HFPU of "aged" white hairs from either African American or Caucasian individuals are practically devoid of pigment (**Figure 1D**), which is consistent with the finding of previous studies[20]. Whereas dark hairs contain melanosomes dispersed throughout the hair medulla when observed by electron microscopy, white hairs from the same individuals show a near complete (>98%) depletion of melanosomes, with the few retained melanosomes, when present, being smaller and less dense (**Figure 1E-I**, see **Supplemental Figure S1** for high-resolution images of mature melanosomes). The digitization of HPPs thus reflects the presence of melanosomes within the HS, and rapid graying events are marked by the loss of melanosomes.

Proteomic alterations in white hairs

To gain molecular insight into the graying process, we performed a comprehensive proteomic analysis comparing dark and white HS. Optimized protein extraction and LC-MS/MS methods were used to process the unusually resistant proteinaceous matrix of the hair shaft and to handle the overly abundant keratin proteins over other potential proteins of interest (see Methods for details). Two independent experiments were performed. *Experiment 1*: matched dark and white hairs collected at the same time from two closely age- and diet-matched individuals (1 female and 1 male, both 35 years old, each dark and white HS measured twice, total n=8); and *Experiment 2 (validation):* n=17 hair segments from 7 different individuals (4 females and 3 males).

In the first experiment, we were able to extract and quantify 323 proteins (>75% of samples) from single 2 cm-long HS segments. Compared to dark HS collected at the same time from the same individuals, white hairs contained several differentially enriched (upregulated) or depleted (downregulated) proteins (**Figure 1J-K** see **Supplemental Table S1** for complete list) on which we performed GO (Gene Ontology) and KEGG (Kyoto Encyclopedia of Genes and Genomes) enrichment analysis, and explored their protein-protein interaction networks (**Supplemental Figure S2**). The protein networks for both downregulated (<0.8-fold, n=23) and upregulated (>1.5-fold, n=67) proteins contain significantly more interactions than expected by chance (P<0.00001, observed vs expected protein-protein interactions). Thus, coherent groups of functionally related proteins are differentially expressed in white hairs, from which two main patterns emerged.

The first main pattern relates to protein biosynthesis and energy metabolism. A large fraction (34.3%) of upregulated proteins in white hairs relate to ribosome function, protein

4

processing, and associated cytoskeletal proteins. Upregulation of the machinery responsible for protein synthesis and amino acid metabolism also included the ribosomal protein RPS15A, which is known to localize to mitochondria. Of all upregulated proteins in white hairs, 26.8% were known mitochondrial proteins (MitoCarta2.0 and others)[21] involved in various aspects of energy metabolism, including substrate transport (carnitine palmitoyltransferase 1A, CPT1A; malonate dehydrogenase 1, MDH1), respiratory chain function (Complex III subunit 1, UQCRC1), and catecholamine homeostasis (Catechol-O-Methyltransferase, COMT). White hairs also contained more proteins involved in glucose (glucose 6-phosphate dehydrogenase, G6PD; phosphoglycerate kinase 1, PGK1) and lipid metabolism located in either mitochondria or cytoplasm (fatty acid synthase, FASN; acyl-CoA thioesterase 7, ACOT7; mitochondrial trifunctional enzyme subunit beta, HADHB) or in peroxisomes (acyl-CoA acyltransferase 1, ACAA1). The metabolic remodeling in white hairs is consistent with the established role of mitochondria and metabolic regulation of hair maintenance in animal models[22-25], and possibly consistent with hair anomalies reported in human patients with mitochondrial disease[26].

A second less robust pattern relates to hair pigmentation. Consistent with the lysosomal origin of melanosomes that are largely absent in depigmented HS[19], several lysosomal proteins (PLD3, CTSD, HEXB, and LAMP1) were downregulated in white hairs. White hairs also showed a depletion of six main keratins (see **Figure S2**), of proteins associated with extracellular secretion (potentially involved with the secretion of melanosomes from melanocytes to keratinocytes), as well as proteins associated with mitochondrial calcium transmembrane transport recently demonstrated to be necessary for melanin pigment production in melanocytes[27].

Finally, white hairs also showed upregulation of antioxidant proteins, specifically those localized to mitochondria and cytoplasm (superoxide dismutase 1, SOD1; peroxiredoxin 2, PRDX2), in line with the role of oxidative stress in HS depigmentation[8,28]. Alterations among these individual metabolic and mitochondrial enzymes were further reflected in KEGG pathways functional enrichment analyses indicating a significant enrichment of metabolic pathways including carbon metabolism and fatty acids, amino acids, and oxidative phosphorylation (see below).

Validation of graying-associated proteomic signatures

To independently validate these results, we extended this analysis to white and dark HS from 6 individuals (3 males, 3 females, range: 24-39 years) analyzed on a separate proteomic platform, in a different laboratory. In this experiment, a total of 192 proteins (≥3 samples) were

quantified from 1cm-long HS segments. This dataset showed a similar trend as the first analysis towards a preferential overexpression of proteins with graying (55% upregulated vs 29% downregulated in white HS) (**Figure 1L-M,** see **Supplemental Table S2** for a complete list). The most highly upregulated proteins included mitochondrial components such as the voltage-dependent anion channel 1 (VDAC1), a subunit of ATP synthase (ATP5A1), and a regulator of mitochondrial respiratory chain assembly (Prohibitin-2, PHB2). Again, the antioxidant enzyme SOD1 was enriched in white relative to dark HS. As a whole, upregulated proteins formed a coherent protein-protein interactions cluster (p<0.00001) and pathway analysis showed a significant enrichment of carbon metabolism, glycolysis/glucogenesis, pyruvate metabolism, and amino acid synthesis pathways in white relative to dark HS (**Supplemental Figure S3, Figure 4E**). On the other hand, proteins downregulated in white hairs were related to cholesterol metabolism, complement-coagulation cascades, and secretory processes shared with immune/inflammatory pathways (**Figure 4E**). The downregulation of secretory pathways is again consistent with the loss of transfer of pigmented melanosomes from the melanocytes to the keratinocytes.

To verify the robustness of these findings using an alternative analytical approach, we built a simple partial least square discriminant analysis (PLS-DA) multivariate model, which provided adequate separation of white vs dark HS (**Supplemental Figure S4**). Simple interrogation of this model to extract the features (i.e., proteins) that maximally contribute to group separation yielded a set of proteins enriched for estrogen signaling pathways, complement and coagulation cascades, as well as metabolic pathways including NAD/NADH, cholesterol, pyruvate, and carbon metabolism, similar to results above. Interestingly, we also identified 13 proteins that were undetectable in any of the dark HS (either not expressed, or below the detection limit), but consistently present in white HS (**Supplemental Table S3**). These proteins are either newly induced or experience a substantial upregulation with graying (fold change tending towards infinity). A separate functional enrichment analysis for these proteins also showed significant enrichment for the same aging-related metabolic pathways as for the complete upregulated protein list: glycolysis/glucogenesis, carbon, pyruvate, and cysteine and methionine metabolism (all P<0.001).

These converging novel proteomics data support a multifactorial etiology directly implicating metabolic changes in human hair graying[2]. Moreover, given that metabolic pathways are rapidly and extensively remodeled by environmental and neuroendocrine factors – i.e., they

6

naturally exhibit plasticity – these data provided the first proteomic evidence that human hair graying could by nature be, at least in part, reversible.

Human hair graying is reversible

Remarkably, our analysis of HPPs in healthy unmedicated individuals revealed a phenomenon whereby white hairs naturally revert to their former dark pigmented state. This had only previously been reported as synchronous heterochromia in two isolated case reports. Here we document the reversal of graying along the same HS in both female and male individuals, ranging from prepubescent children to adults (age range 9 to 39 years), and across individuals of different ethnic backgrounds (Hispanic, Caucasian, Asian, African American). This phenomenon was observed across frontal, temporal, and parietal regions of the scalp (**Figure 2A**). We also document reversal of HS graying across other corporeal regions, including pubic (**Figure 2B**) and beard hairs (**Figure 2C**). The existence of white HS undergoing repigmentation across ages, sexes, ethnicity, and corporeal regions documents the reversibility of hair graying as a general phenomenon not limited to scalp hairs.

Moreover, more complex HPPs with double transitions and reversions in the same HS were also observed in both directions: HS undergoing graying followed by rapid reversal (**Figure 2D**), and repigmentation rapidly followed by graying (**Figure 2E**). Importantly, both patterns must have occurred over the course of a single follicular growth cycle, implicating cellular mechanisms within the HFPU. To our knowledge, this represents the first generalizable and quantitative account of the natural reversibility of hair graying in humans.

We understand the emergence of a reverted HS – that is, a HS with a white distal segment but with a dark proximal end – as necessarily having undergone repigmentation to its original state following a period (of unknown duration) as a depigmented "old" white hair (**Figure 2F**). In double transition HS with three segments, repigmentation must take place within weeks to months after graying has occurred, producing three distinct segments present on the same hair strand (**Figure 2G**). Microscopic imaging along the length of a single HS undergoing a double transition (graying followed by rapid reversal) can be visualized in **Video S1**, illustrating the dynamic loss and return of pigmented melanosomes within the same HS.

Our hair digitization approach also provides the first estimates of the rates of change in pigmentation for HS covering a broad range of initial colors and darkness (**Figure 2H**). Across individuals, assuming a hair growth rate of 1cm/month[16], the rates of depigmentation in graying

hairs range from 0.3 to 23.5 units of hair optical density (scale of 0-255) per day, corresponding to between 0.2% and 14.4% loss of hair color per day (**Figure 2I**). The rate at which HS regain pigmentation during reversal was 0.1 to 42.5 units per day, which is similar (~30% faster on average) to the rate of graying (Cohen's d = 0.15, p = 0.59) (**Figure 2J**). Given these rates, the fastest measured transitioning hairs gray and undergo reversal in ~3-7 days (median: ~3 months). Thus, rather than progressively drifting back towards the original color, repigmentation of white human HS occurs within the same time frame and at least as rapidly as the process of graying itself. **Supplemental Figure S5** shows the spectrum of graying transitions and reversals patterns observed in our cohort, including measured rates of repigmentation along individual hairs. These data suggest that reversal/repigmentation may reflect the action of as yet unknown local or systemic factors acting on the HFPU within a time frame of days to weeks.

Multiple scalp hairs exhibit synchronous behavior

We then asked whether the reversal of graying is governed by a process that is unique to each human scalp HF or if it is coordinated by systemic factors that simultaneously affect multiple HFs. Participants' scalps were visually inspected to identify two-colored hairs, including both graying transitions and reversal. In our combined cohort, three individuals had multiple two-colored hairs collected within a one-month interval. In each case, the multiple two-colored hairs originated from independent HFs separated by at least several centimeters (e.g., left vs right temporal, or frontal vs temporal). In a first 35-year-old female participant, 3 two-colored hairs were identified at a single instance of collection. All exhibited dark-to-white graying. Strikingly, when the HPP was quantified and plotted the 3 hairs showed unusual synchrony with each other, following similar graying trajectories as measured by their correlation (p=0.069, **Figure 3A**) and suggesting that their behavior across months was related. In a 37-year-old female participant, two transition hairs were identified. Again, the HPPs for both hairs revealed similar trajectories, in this case undergoing spontaneous reversal in a near-synchronous manner upon alignment (p<0.001, **Figure 3B**). The coordinated graying and reversal dynamics among multiple non-adjacent HS from the same individuals suggests the existence of systemic factors that influence all HFs simultaneously and regulate HPPs in sensitive hairs.

Candidate systemic hair pigmentation modulators include neuropeptides, redox balance, and steroid or catecholamine hormones[5,15,29] that can directly regulate the human HFPU[2], impact intrafollicular clock activity[29], or regulate the expression of other melanotropic neurohormones in the human HFPU such as α-MSH, ß-endorphin, and TRH[30]. These factors

8

must act in parallel with genetic factors that influence inter-individual differences in aging trajectories.

Hair graying and reversal are linked to stress levels

In light of these results, we next applied our HPP platform to examine the possibility that psychological stress is associated with hair graying/reversal in humans. Anecdotal case reports suggest that psychological stress and other behavioral factors accelerate the hair graying process[31], a notion recently supported by preclinical evidence demonstrating that adrenergic signaling by norepinephrine signaling leads to melanocyte stem cell depletion in mice[5]. However, contrary to mice where this process is irreversible, our data demonstrates that human hair graying is, at least under some circumstances, reversible. This highlighted a fundamental difference between rodent and human HF biology, calling for a quantitative examination of this process in humans.

As evidence that environmental or behavioral factors influence human hair graying, epidemiological data suggests that smoking and greater perceived life stress is associated with premature graying[32]. Chronic psychosocial stress also precipitates telomere shortening, DNA methylation-based epigenetic age, as well as other biological age indicators in humans[4,33], demonstrating that psychological factors can measurably influence human aging biology. To test the hypothesis that psychosocial or behavioral factors would also influence graying at the single-HF level, we leveraged the fact that HPPs reflect longitudinal records of growth over time (similar to tree rings), which can be aligned with assessments of life stress exposures over the past year. By converting units of hair length into time, perceived stress levels can be quantitatively mapped onto HPPs in both graying and transitional hairs.

A systematic survey of two-colored hairs on the scalp of a 35-year-old Caucasian male over a two-day period yielded five two-colored HS from the frontal and temporal regions of the scalp. Interestingly, all HS exhibited reversal. HPP analysis further showed that all HS underwent reversal of graying around the same time period. We therefore hypothesized that the onset of the reversal would coincide with a decrease in perceived life stress. A retrospective assessment of stress levels (time-anchored visual analog scale, see *Methods* and **Supplemental Figure S6** for details) was then compared to the HPPs. The reversal of graying for all hairs coincided closely with the decline of stress and a 1-month period of lowest stress over the past year (0 on a scale of 0-10, from a two-week vacation) (**Figure 3C**).

We were also able to examine a two-colored hair characterized by an unusual pattern of complete HS graying followed by rapid and complete reversal (same as in Figure 2B) plucked from the scalp of a 30-year-old Asian female participant. HPP analysis of this HS showed a graying segment representing approximately 2 cm. We therefore hypothesized that this reversible graying event would coincide with a temporary increase in life stress over the corresponding period. Strikingly, the quantitative life stress assessment over the last year revealed a specific 2-month period associated with objective life stressors (marital conflict and separation, relocation) where the participant rated her perceived stress as the highest (9-10 out of 10) over the past year. The increase in stress corresponded in time with the complete but reversible hair graying (**Figure 3D**). This relationship was highly significant (p=0.007) based on our permutation test. Given the low statistical probability that these events are related by chance, life stress is the likely preceding cause of these HS graying and reversal dynamics.

Single-hair longitudinal proteomic signature

To assess whether rapid graying and reversal events among a single hair are molecularly similar or distinct to those described above, we dissected 6 segments (2 dark, 2 white, 2 reverted) of the single HS in Figure 3D and quantified their proteomes. This produced a longitudinal, single-hair, proteomic signature (**Figure 3E**) containing 301 proteins quantified in ≥2 segments. To examine how the proteome as a whole is altered through the graying and reversal transitions associated with stress levels, we generated a PLS-DA model with all 6 segments. Both dark segments clustered together, with similar values on both first and second principal components. The white and reverted segments clustered in separate topological spaces (**Figure 3F**). Graying was associated with a positive shift largely along the first component (Component 1), whereas reversal was associated with a negative shift on the second component (Component 2) and a more modest negative shift in Component 1. We therefore extracted loading weights of each protein on Components 1 and 2 (reflecting each protein's contribution to group separation) and used the top proteins (n=20 highest negative and 20 positive loadings, total n=40 per component) to interrogate KEGG and GO databases.

The model's Component 1 (associated with graying) contained proteins that were either i) not expressed in the dark HS but induced selectively in the white HS segment, or ii) highly abundant in dark segments but strongly downregulated in white and reverted segments (**Figure 3H**, *top* and *bottom*, respectively). In gene set enrichment analysis of Component 1 (graying), the top three functional categories were carbon metabolism, glycolysis/gluconeogenesis, and Kreb's cycle (**Figure 4E**). Component 2 (reversal)-associated proteins exhibited distinct

10

trajectories either peaking in the first white segment or upon reversal (**Figure 3I**) and mapped to pathways related to the complement activation cascade, infectious processes, and Parkinson's and Huntington's disease (**Figure 4E**). In contrast, a null set of hair proteins not contributing to either components exhibited enrichment for extracellular exosomes and cell-cell adhesion that reflect hair shaft biology (Supplemental Figure S7), therefore illustrating the specificity of our findings related to graying and reversal. These data indicate that the reversal of graying at the single-hair level is not associated with a complete reversal in the molecular composition of the HS. Rather, some of the proteomic changes in hair graying are enduring despite successful repigmentation.

Shared proteomic signatures of hair graying

To systematically examine the overlap among the different proteomic datasets and derive functional insight into the hair graying process in humans, we then integrated results from the three datasets described above. White HS show consistently more upregulated than downregulated proteins across datasets (2.91-fold in Experiment 1, 1.89-fold in Experiment 2) (**Figure 4A**). This preferential upregulation suggests that the depigmentation process likely involves active metabolic remodeling rather than a passive loss of some pigmentation-related factor. The overlap in the specific proteins identified across dark-white comparisons and among the 6-segments hair is illustrated in **Figure 4B**.

Five proteins were consistently upregulated between experiments 1 and 2. These include three well-defined resident mitochondrial proteins involved in lipid metabolism: CPT1A, which imports fatty acids in mitochondria; ACOT7, which hydrolyzes long-chain fatty acyl-CoA esters in the mitochondrial matrix and cytoplasm; and SOD1, which dismutates superoxide anion into hydrogen peroxide (H_2O_2) in the mitochondrial intermembrane space. The other two proteins include the actin-depolymerizing protein cofilin-1 (CFL1) and the core glycolysis enzyme phosphoglycerate kinase 1 (PGK1) (**Figure 4C**). Interestingly, CFL1 promotes mitochondrial apoptotic signaling via cytochrome c release[34] and regulates mitochondrial morphology via its effect on actin polymerization-dependent mitochondrial fission[35]. Moreover, although PGK1 is a cytoplasmic kinase, it was recently demonstrated to translocate inside mitochondria where it phosphorylates and inhibits pyruvate dehydrogenase and Krebs cycle activity[36]. Thus, all five proteins validated across both experiments are linked to mitochondrial energy metabolism, implicating mitochondrial remodeling as a feature of hair graying. Interestingly, all five proteins have also been linked to the biology of melanocytes[37-41], which produce pigment in the HFPU. Together, these data suggest that HS proteome profiling may

11

provide a retrospective access to some aspect of melanocyte metabolism, which opens new possibilities to study HF aging biology. The downregulated proteins were keratins, with small effect sizes, and not particularly robust.

We note that since the observed proteomic signatures are related to specific metabolic pathways rather than the typical high-abundance mitochondrial housekeeping proteins, we reasoned that the upregulation of these mitochondrial components unlikely reflects a bulk increase in total mitochondrial content. To investigate this point using an independent method, we quantified mitochondrial DNA (mtDNA) abundance in human HS by real-time qPCR. Both white and dark HS contain surprisingly and similarly high levels of mtDNA (**Figure 4D**). The same was true in the bulbs of the same hairs (**Supplemental Figure S8**). High mitochondrial genome abundance in the HS supports the high abundance of mitochondrial proteins in HS in general. In relation to graying, the similar mtDNA levels between dark and white hairs increases the likelihood that the proteomic changes reflect the induction of specific metabolic pathways associated with hair graying rather than bulk increase in mitochondrial mass.

Finally, to identify a general proteomic signature of graying hair, we compiled the enrichment scores for KEGG pathways across all datasets (**Figure 4E**). Consistent with the function of the individual proteins mentioned above, across both group comparisons and the multi-segment double-transition hair, white HS showed consistent upregulation of carbon metabolism and amino acid biosynthesis, as well as glycolysis/gluconeogenesis and general metabolic pathways. Comparatively fewer pathways were consistently represented for downregulated proteins across independent experiments. In relation to hair biology, our data also provides a quantitative map of the co-expression among keratin and non-keratin HS proteins across dark and white hairs (**Figure 4F**). Computing the cross-correlations for each protein pair revealed four main clusters among the hair proteome . As expected for hair, keratins were well-represented and constituted the main GO biological processes category for 3 of the 4 clusters. The top KEGG categories included glycolysis and estrogen signaling pathways, which also showed strong co-expression with each other, highlighting potential interaction among endocrine and metabolic processes in relation to human hair pigmentation. In general, the identification of several non-keratin metabolism-related proteins in the HS opens new opportunities to investigate graying pathobiology and to non-invasively access past molecular and metabolic changes that have occurred in the aging HFPU of the growing hair.

In silico modeling of hair graying and reversal

Finally, to narrow the range of plausible mechanisms for the observed age-related graying and reversal events, we developed a simulation model of HPPs. Graying dynamics of an individual's hair population (~100,000 hairs) across the average 80-year lifespan cannot practically be measured. In the absence of such data, we propose here a mathematical model to simulate hair graying trajectories across the human lifespan (**Figure 5A**, available online, see *Methods* for details) as has been attempted previously for hair growth cycles[42]. As basic tenets for this model, it is established that *i)* the onset of human hair graying is delayed and very rarely begins in childhood, *ii)* graying routinely starts between 20-50 years of age, *iii)* graying is progressive in nature (the total number and percentage of gray hairs increases over time), and *iv)* graying typically reaches close to 100% white hairs in old age[9]. Additionally, our findings demonstrate that *v)* age-related graying is naturally reversible, at least temporarily, and may be acutely triggered by stressful life experiences, the removal of which can trigger reversal.

Aiming for the simplest model that accounts for these known features of hair graying dynamics, we found a satisfactory model with three components (**Figure 5B**): 1) an "*aging factor*" that progressively accumulates within each hair follicle, based on the fact that biological aging is more accurately modeled with the accumulation of damage, rather than decline in some reserve[43]; 2) a biological *threshold*, beyond which hairs undergo depigmentation (i.e., graying), characterizing the transition between the dark and white states in the same HS; and 3) a "*stress factor*" that acutely but reversibly increases the aging factor during a stressful event. For modeling purposes, the accumulation of the aging factor is equivalent to the inverse of the decrease in a youth factor (e.g., loss of telomere length with age). Based on our data indicating that not all hairs are in perfect synchrony, the proposed model for an entire population of hairs must also allow a variety of aging rates, as well as differential sensitivity to stress among individual hairs.

We find that the model's predicted hair population behavior (% of white HSs on a person's head over time) across the lifespan is consistent with expected normal human hair graying dynamics (**Figure 5C**). White hairs are largely absent until the onset of graying past 20 years of age then accumulate before finally reaching a plateau near 100 years. Thus, this model appears to recapitulate the expected between-hair heterogeneity of graying within an individual. There are also inter-individual differences in the rate of graying: some individuals begin graying early (onset in early 20's); some begin late (onset in 50's). A higher rate of accumulation of the aging factor (higher slope for each hair) or a lower threshold naturally accounts for earlier onset of graying. In addition, our model reveals that within a person, greater hair-to-hair heterogeneity

13

in the rate of aging between HFs, modeled as the standard deviation of slope across hairs, also influences the onset of graying. Greater heterogeneity between HFs produces earlier onset of graying, whereas decreasing hair-to-hair variation (i.e., lower heterogeneity) is associated with a "youthful" later onset of graying (**Figure 5D**). Interestingly, this unpredicted result aligns with the notion that increased cell-to-cell heterogeneity is a conserved feature of aging[44-46], and that hematological heterogeneity predicts all-cause mortality in humans[47].

Modeling stressors produce hair graying and temporary reversal

Using parameter values that yield the average onset and rate of graying, we then simulated the influence of acute stressors, either early in life before the onset of graying, or later once gray HSs have begun to accumulate. Similar to our data, the model also predicts transitory events of graying (e.g., graying followed by reversal, see Figure 3D). Transitory graying events do not affect all hairs, only those that are close to the threshold at the time of stress exposure undergo graying, whereas hairs whose cumulative aging factors are substantially lower than threshold do not show stress-induced graying (a 5-year-old is unlikely to get gray hairs from stress, but a 45-year-old can) (**Figure 5E-F**). Gray hairs far above threshold are not affected by periods of stress. Thus, our model accounts for both the overall hair graying dynamics across the lifespan, and how a stressor (or its removal) may precipitate (or cause reversal of) graying in hairs whose aging factor is close to the graying threshold.

We speculate that this simulation opens an attractive possibility whereby HPP data from individuals could be used in models to formulate predictions about future graying trajectories, and to use HPPs and hair population graying behavior to track the effectiveness of behavioral and/or therapeutic interventions aimed at modifying human aging. Extending our high-resolution quantitative digitization approach to hundreds of randomly sampled dark non-transitioning hairs from different scalp regions in the same individuals, we also show that fully dark (i.e., non-graying) HSs exhibit unique HPPs, and that different scalp regions may exhibit different average HPPs, providing a foundation for future studies (**Figure S9**). This regional segregation may reflect well-recognized regional differences in the rate of HS formation[48]. Thus, future models may also be able to leverage information contained within HPPs from non-graying hairs and make specific inference from hairs collected across scalp regions. Similar to how decoding temporal patterns of electroencephalography (EEG) provides information about the state of the brain, it is imaginable that decoding HPP analysis may provide information about the psychobiological state of the individual.

Discussion

Our approach to quantify HPPs demonstrates rapid graying transitions and their natural reversal within individual human hair follicles over a much shorter time span and at a higher frequency than had previously been appreciated. The proteomic features of hair graying directly implicate metabolic pathways that are both reversible in nature, and sensitive to stress-related neuroendocrine factors. This result provides a plausible biological basis for the reversibility of graying and its association with psychological factors, and also supports the possibility that this process could be targeted pharmacologically. The upregulation of specific components of mitochondrial energy metabolism in white hairs suggests that metabolism regulates not only hair growth as previously demonstrated[22,49,50], but also HS pigmentation. Energy metabolism is a major contributor to other disease-related aging features[51], including lifespan regulation[52]. Quantitative biological age indicators such as telomere length[53] and DNA methylation[54] have also recently been demonstrated to exhibit temporary reversal in response to exercise and dietary interventions. Along with these findings, our data strongly support the notion that human aging is not a linear and irreversible biological process and may, at least in part, be halted or even reversed. Our method to map the rapid (weeks to months) and natural reversibility of human hair graying may thus provide a powerful model to explore the malleability of human aging within time scales substantially smaller than the human lifespan.

In relation to psychobiological processes, the spatio-temporal resolution of the HPP approach also provides investigators with an instructive new research tool that allows to link hair graying and reversal events with psychosocial exposures at an unprecedented level of resolution. Here we provided proof-of-concept evidence that biobehavioral factors are closely linked to human hair graying dynamics. Our optical digitization approach thus extends previous attempts to extract temporal information from human hairs and illustrate the utility of HPP profiling as an instructive and sensitive psychobiology research model, possibly allowing to visualize and retrospectively quantify the biological embedding of life exposures at different stages of the lifespan.

References

1   Tobin, D. J. The cell biology of human hair follicle pigmentation. *Pigment cell & melanoma research* **24**, 75-88, doi:10.1111/j.1755-148X.2010.00803.x (2011).

2   Paus, R. A neuroendocrinological perspective on human hair follicle pigmentation. *Pigment cell & melanoma research* **24**, 89-106, doi:10.1111/j.1755-148X.2010.00808.x (2011).

3   Puterman, E. *et al.* Lifespan adversity and later adulthood telomere length in the nationally representative US Health and Retirement Study. *Proc Natl Acad Sci U S A* **113**, E6335-E6342, doi:10.1073/pnas.1525602113 (2016).

4   Epel, E. S. *et al.* Accelerated telomere shortening in response to life stress. *Proc Natl Acad Sci U S A* **101**, 17312-17315, doi:0407162101 [pii]10.1073/pnas.0407162101 (2004).

5   Zhang, B. *et al.* Hyperactivation of sympathetic nerves drives depletion of melanocyte stem cells. *Nature* **577**, 676-681, doi:10.1038/s41586-020-1935-3 (2020).

6   Panhard, S., Lozano, I. & Loussouarn, G. Greying of the human hair: a worldwide survey, revisiting the '50' rule of thumb. *Br J Dermatol* **167**, 865-873, doi:10.1111/j.1365-2133.2012.11095.x (2012).

7   Nishimura, E. K., Granter, S. R. & Fisher, D. E. Mechanisms of hair graying: incomplete melanocyte stem cell maintenance in the niche. *Science* **307**, 720-724, doi:10.1126/science.1099593 (2005).

8   Arck, P. C. *et al.* Towards a "free radical theory of graying": melanocyte apoptosis in the aging human hair follicle is an indicator of oxidative stress induced tissue damage. *FASEB J* **20**, 1567-1569, doi:10.1096/fj.05-4039fje (2006).

9   Trueb, R. M. & Tobin, D. J. *Aging Hair*. (Springer, 2010).

10   Komagamine, T., Suzuki, K. & Hirata, K. Darkening of white hair following levodopa therapy in a patient with Parkinson's disease. *Mov Disord* **28**, 1643, doi:10.1002/mds.25696 (2013).

11   Reynolds, N. J., Crossley, J., Ferguson, I. & Peachey, R. D. Darkening of white hair in Parkinson's disease. *Clin Exp Dermatol* **14**, 317-318, doi:10.1111/j.1365-2230.1989.tb01992.x (1989).

12   Ricci, F., De Simone, C., Del Regno, L. & Peris, K. Drug-induced hair colour changes. *Eur J Dermatol* **26**, 531-536, doi:10.1684/ejd.2016.2844 (2016).

13   Sieve, B. F. Clinical Achromotrichia. *Science* **94**, 257-258, doi:10.1126/science.94.2437.257 (1941).

14   Yoon, K. H., Kim, D., Sohn, S. & Lee, W. S. Segmented heterochromia in scalp hair. *J Am Acad Dermatol* **49**, 1148-1150, doi:10.1016/s0190-9622(03)00471-7 (2003).

15   Paus, R., Langan, E. A., Vidali, S., Ramot, Y. & Andersen, B. Neuroendocrinology of the hair follicle: principles and clinical perspectives. *Trends Mol Med* **20**, 559-570, doi:10.1016/j.molmed.2014.06.002 (2014).

16   LeBeau, M. A., Montgomery, M. A. & Brewer, J. D. The role of variations in growth rate and sample collection on interpreting results of segmental analyses of hair. *Forensic Sci Int* **210**, 110-116, doi:10.1016/j.forsciint.2011.02.015 (2011).

17   Douglass, A. E. in *Climatic Cycles and Tree Growth* Vol. vol. II. (Carnegie Institute of Washington, 1928).

18   Paus, R. & Cotsarelis, G. The biology of hair follicles. *N Engl J Med* **341**, 491-497, doi:10.1056/NEJM199908123410706 (1999).

19   Slominski, A. *et al.* Hair follicle pigmentation. *The Journal of investigative dermatology* **124**, 13-21, doi:10.1111/j.0022-202X.2004.23528.x (2005).

20   Cho, S. B., Zheng, Z., Kim, J. Y. & Oh, S. H. Segmented heterochromia in a single scalp hair. *Acta Derm Venereol* **94**, 609-610, doi:10.2340/00015555-1790 (2014).

21   Calvo, S. E., Clauser, K. R. & Mootha, V. K. MitoCarta2.0: an updated inventory of mammalian mitochondrial proteins. *Nucleic Acids Res* **44**, D1251-1257, doi:10.1093/nar/gkv1003 (2016).

22   Flores, A. *et al.* Lactate dehydrogenase activity drives hair follicle stem cell activation. *Nat Cell Biol* **19**, 1017-1026, doi:10.1038/ncb3575 (2017).

23   Singh, B., Schoeb, T. R., Bajpai, P., Slominski, A. & Singh, K. K. Reversing wrinkled skin and hair loss in mice by restoring mitochondrial function. *Cell Death Dis* **9**, 735, doi:10.1038/s41419-018-0765-9 (2018).

24   Vidali, S. *et al.* Hypothalamic-pituitary-thyroid axis hormones stimulate mitochondrial function and biogenesis in human hair follicles. *The Journal of investigative dermatology* **134**, 33-42, doi:10.1038/jid.2013.286 (2014).

25   Kloepper, J. E. *et al.* Mitochondrial function in murine skin epithelium is crucial for hair follicle morphogenesis and epithelial-mesenchymal interactions. *The Journal of investigative dermatology* **135**, 679-689, doi:10.1038/jid.2014.475 (2015).

26   Silengo, M. *et al.* Hair anomalies as a sign of mitochondrial disease. *Eur J Pediatr* **162**, 459-461, doi:10.1007/s00431-003-1228-5 (2003).

27   Zhang, Z., Gong, J., Sviderskaya, E. V., Wei, A. & Li, W. Mitochondrial NCKX5 regulates melanosomal biogenesis and pigment production. *J Cell Sci* **132**, doi:10.1242/jcs.232009 (2019).

28   Wood, J. M. *et al.* Senile hair graying: H2O2-mediated oxidative stress affects human hair color by blunting methionine sulfoxide repair. *FASEB J* **23**, 2065-2075, doi:10.1096/fj.08-125435 (2009).

29   Hardman, J. A. *et al.* The peripheral clock regulates human pigmentation. *The Journal of investigative dermatology* **135**, 1053-1064, doi:10.1038/jid.2014.442 (2015).

30   Gaspar, E. *et al.* Thyrotropin-releasing hormone selectively stimulates human hair follicle pigmentation. *The Journal of investigative dermatology* **131**, 2368-2377, doi:10.1038/jid.2011.221 (2011).

31   Nahm, M., Navarini, A. A. & Kelly, E. W. Canities subita: a reappraisal of evidence based on 196 case reports published in the medical literature. *Int J Trichology* **5**, 63-68, doi:10.4103/0974-7753.122959 (2013).

32   Akin Belli, A., Etgu, F., Ozbas Gok, S., Kara, B. & Dogan, G. Risk Factors for Premature Hair Graying in Young Turkish Adults. *Pediatr Dermatol* **33**, 438-442, doi:10.1111/pde.12881 (2016).

33   Han, L. K. M. *et al.* Accelerating research on biological aging and mental health: Current challenges and future directions. *Psychoneuroendocrinology* **106**, 293-311 (2019).

34   Hoffmann, L., Rust, M. B. & Culmsee, C. Actin(g) on mitochondria - a role for cofilin1 in neuronal cell death pathways. *Biol Chem* **400**, 1089-1097, doi:10.1515/hsz-2019-0120 (2019).

35   Rehklau, K. *et al.* Cofilin1-dependent actin dynamics control DRP1-mediated mitochondrial fission. *Cell Death Dis* **8**, e3063, doi:10.1038/cddis.2017.448 (2017).

17

36   Nie, H. *et al.* O-GlcNAcylation of PGK1 coordinates glycolysis and TCA cycle to promote tumor growth. *Nat Commun* **11**, 36, doi:10.1038/s41467-019-13601-8 (2020).

37   Sung, G. J. *et al.* Targeting CPT1A enhances metabolic therapy in human melanoma cells with the BRAF V600E mutation. *Int J Biochem Cell Biol* **81**, 76-81, doi:10.1016/j.biocel.2016.10.019 (2016).

38   Sumantran, V. N., Mishra, P. & Sudhakar, N. Microarray analysis of differentially expressed genes regulating lipid metabolism during melanoma progression. *Indian J Biochem Biophys* **52**, 125-131 (2015).

39   Oh, C. T. *et al.* Superoxide dismutase 1 inhibits alpha-melanocyte stimulating hormone and ultraviolet B-induced melanogenesis in murine skin. *Ann Dermatol* **26**, 681-687, doi:10.5021/ad.2014.26.6.681 (2014).

40   Bracalente, C. *et al.* Cofilin-1 levels and intracellular localization are associated with melanoma prognosis in a cohort of patients. *Oncotarget* **9**, 24097-24108, doi:10.18632/oncotarget.25303 (2018).

41   Morvan, D., Steyaert, J. M., Schwartz, L., Israel, M. & Demidem, A. Normal human melanocytes exposed to chronic insulin and glucose supplementation undergo oncogenic changes and methyl group metabolism cellular redistribution. *Am J Physiol Endocrinol Metab* **302**, E1407-1418, doi:10.1152/ajpendo.00594.2011 (2012).

42   Halloy, J., Bernard, B. A., Loussouarn, G. & Goldbeter, A. Modeling the dynamics of human hair cycles by a follicular automaton. *Proc Natl Acad Sci U S A* **97**, 8328-8333, doi:10.1073/pnas.97.15.8328 (2000).

43   Kinzina, E. D., Podolskiy, D. I., Dmitriev, S. E. & Gladyshev, V. N. Patterns of Aging Biomarkers, Mortality, and Damaging Mutations Illuminate the Beginning of Aging and Causes of Early-Life Mortality. *Cell Rep* **29**, 4276-4284 e4273, doi:10.1016/j.celrep.2019.11.091 (2019).

44   Bahar, R. *et al.* Increased cell-to-cell variation in gene expression in ageing mouse heart. *Nature* **441**, 1011-1014, doi:10.1038/nature04844 (2006).

45   Enge, M. *et al.* Single-Cell Analysis of Human Pancreas Reveals Transcriptional Signatures of Aging and Somatic Mutation Patterns. *Cell* **171**, 321-330 e314, doi:10.1016/j.cell.2017.09.004 (2017).

46   Martinez-Jimenez, C. P. *et al.* Aging increases cell-to-cell transcriptional variability upon immune stimulation. *Science* **355**, 1433-1436, doi:10.1126/science.aah4115 (2017).

47   Patel, K. V. *et al.* Red cell distribution width and mortality in older adults: a meta-analysis. *J Gerontol A Biol Sci Med Sci* **65**, 258-265, doi:10.1093/gerona/glp163 (2010).

48   Robbins, C. R. *The Chemical and Physical Behavior of Human Hair*. (Springer, 2012).

49   Mancino, G. *et al.* The Thyroid Hormone Inactivator Enzyme, Type 3 Deiodinase, Is Essential for Coordination of Keratinocyte Growth and Differentiation. *Thyroid*, doi:10.1089/thy.2019.0557 (2020).

50   Ramot, Y. *et al.* Spermidine promotes human hair growth and is a novel modulator of human epithelial stem cell functions. *PLoS One* **6**, e22564, doi:10.1371/journal.pone.0022564 (2011).

51   Kennedy, B. K. *et al.* Geroscience: linking aging to chronic disease. *Cell* **159**, 709-713, doi:10.1016/j.cell.2014.10.039 (2014).

52   Latorre-Pellicer, A. *et al.* Mitochondrial and nuclear DNA matching shapes metabolism and healthy ageing. *Nature* **535**, 561-565, doi:10.1038/nature18618 (2016).

53   Puterman, E. *et al.* Aerobic exercise lengthens telomeres and reduces stress in family caregivers: A randomized controlled trial - Curt Richter Award Paper 2018. *Psychoneuroendocrinology* **98**, 245-252, doi:10.1016/j.psyneuen.2018.08.002 (2018).

54   Fahy, G. M. *et al.* Reversal of epigenetic aging and immunosenescent trends in humans. *Aging Cell* **18**, e13028, doi:10.1111/acel.13028 (2019).

Methods

Participants

The study was approved by New York State Psychiatric Institute (Protocol #7748). All participants provided written informed consent. Dark, white, and bi-color hairs were collected from healthy participants self-identified as "having some gray hairs" or "two-colored hairs". Exclusion criteria included the use of dye, bleaching, or other chemical treatments on hairs. In addition, participants with hairs shorter than approximately 4 cm were excluded. Participants were recruited via local advertisement and using a snowball recruitment strategy. Eligible participants were asked to provide all two-colored hairs present on their scalps or other body regions. A total of 14 individuals (7 females, 7 males), mean age 35 ± 13 (SD, range: 9-65), were recruited. Hairs were plucked, manually or with standard flat tip tweezers, from the scalp or other body regions and archived for future imaging or molecular analyses. Only hairs with an intact bulb (excluding broken hairs) were used in analyses to enable the interpretation of the direction of pigmentation – transition if the HS tip is dark and the root white, reversal if the HS tip is white and the root dark. Where possible, participants with two-colored hairs also provided fully dark or white hairs for comparison.

Hair imaging

Whole hairs were first photographed using a Panasonic DC-FZ80 Digital Camera against a white background, with the hair tip and bulb systematically oriented. To facilitate visualization of the images of whole hairs in the figures (photographic insets of whole hairs), the exposure, saturation, sharpness and light/dark tones of the photographs were enhanced. For microscopic imaging of hair bulbs and HFPU, individual hair shafts and roots were imaged with an Olympus BX61 upright microscope equipped with a digitized stage (ProScan; Prior Scientific), a 2.5x/0.075 air (Zeiss, Germany), 10x/0.4 air (Zeiss, Germany) or 40x/1.3 oil (Olympus, MA) objectives, using DP71 camera (Olympus, MA) and MetaMorph software (Molecular Devices, CA) version 7.7.7.0. Images were scaled and analyzed in ImageJ (version 1.42q, NIH, http://rsb.info.nih.gov/ij). For microscopic imaging of hair shafts and videos of HPP transitions along the length of hair shafts, hairs were temporarily mounted with water on a glass slide (10x magnification, 15ms exposure, 24-bit, ISO 1600, 4080x3072 digitizer).

Digitization of hair pigmentation patterns

To generate high-resolution hair pigmentation patterns (HPPs), hairs were digitized as high-resolution 8-bit Grayscale images (3,200dpi, default adjustments, Epson Perfection V800 Photo Scanner), and the scanned images were processed using Image J (Fiji). To capture both

the white and dark sections of each hair, hairs were immobilized onto a smooth surface by taping the bulb (proximal to the epidermis) of each hair, straightening the entire length, and taping the tip (distal to epidermis). Areas of each hair between these regions were used for analyses. To extract hair darkness at each point along the length, pixel luminosity at each position was estimated as a minimum of a small 1D range of pixels perpendicular to the shaft axis, where the hair itself represented the darkest area, and a graph was created plotting the intensity in arbitrary units (A.U.) by distance (cm). Intensity ranged from 0-255 A.U., with 0 being white and 255 being black. The data was then denoised using a 100 pixels rolling average, and imported into Prism 8.

To compare intensity profiles across multiple hairs we transformed numerical intensity values by normalizing to the average intensity of each hair. A total of 100 randomly selected dark hairs were manually plucked from one female and one male individual, including 25 hairs per head region (left and right temporal, top, and crown). Digitized hairs for each individual were graphed as a heatmap, grouped by head region. The intensity of all hairs in one region were then averaged to create one 'average' hair from each region, illustrating regional differences. A plot was then made for the four 'average hairs', one from each head region.

Electron microscopy

Dark and white hairs were collected from two healthy individuals; a 38-year-old African American male, a 33-year-old Caucasian male. The African American hairs were expectedly curly, while the Caucasian hairs were straight. Hairs were fixed in a 2% glutaraldehyde solution in 0.1M cacodylate (TAAB Lab Equipment) buffer, pH 7.4 as described previously[55]. Briefly, plucked hair shafts were cut to 2-3cm in length, immersed in fixative, and incubated at room temperature for 2 weeks. HS were then post-fixed and dehydrated in ethanol, cut into smaller segments of 0.5cm, and embedded in longitudinal orientation in 100% resin. Orientation and section quality were confirmed with 1µm-thick sections, and ultrathin sections of 70nm were cut using a diamond knife on a Leica EM UC7 ultramicrotome. Sections mounted on Pioloform filmed copper grids prior to staining with 2% aqueous uranyl acetate and lead citrate (Leica). Ultrathin sections were examined on a Phillips CM 100 Compustage (FEI) transmission electron microscope and digital micrographs were captured by an AMT CCD camera.

Matched dark and white hairs from the donors were imaged, and three different segments along each hair were analyzed. All images used for analysis were captured at 7,500x magnification, with a pixel size of 0.00902um/pixel. Images were imported into ImageJ for analysis and all melanin granules contained within a given picture were manually traced (Intuos

tablet). In each photograph, the intensity of the melanin granules, cortex, and background (outside the hair) were quantified. Cortex and melanin granule intensity were normalized by subtracting the background average intensity (measured from three different standard regions of interest – ROIs) to ensure comparability of various micrographs, hair segments, and between dark and white hairs. The intensity of the cortex was also quantified from eight different ROIs devoid of melanin granules.

To compute melanin granule size, we obtained the surface area of each manually traced granule. To compute melanin granule density per hair region, the total cortex area in each scaled micrograph was recorded and was divided by the total number of granules that were found in that image, yielding the number of granules/um^2, which was then multiplied by 100.

Hair shaft proteomics

Experiment 1: For label-free quantitative proteomics, a 2-cm segment of plucked dark and white HS matched for distance relative to the bulb was isolated from one female and one male participant. Each HS was washed independently in 20% methanol, ground and extracted in a glass homogenizer with SDS in Tris-buffered saline with 150-200ul of 4% protease inhibitor cocktail (Sigma P8340), precipitated with chloroform-methanol, redissolved in 8 M urea with ammonium bicarbonate, reduced, alkylated and digested with trypsin. For liquid chromatography and mass spectrometry two technical replicas (161 min chromatograms) were recorded for each sample. Separations were performed with an Ultimate 3000 RSLCNano (Thermo Scientific) on a 75 µm ID x 50 cm Acclaim PepMap reversed phase C18, 2 µm particle size column. Chromatographic flow rate was 300 nL/min with an acetonitrile/formic acid gradient. The liquid chromatograph was coupled to a Q Exactive HF mass spectrometer (Thermo Scientific) using data-dependent acquisition. Data were searched against a Swiss-Prot human protein database with Mascot v.2.5.1 (Matrix Science Ltd.). Semi-quantitative exponentially-modified protein abundance index (emPAI) was calculated by the Mascot software. A total of 744 proteins were detected. Proteins not detected in two or more samples from a total of 8 were not included for further analyses. Among the eligible proteins (n=323), the fold change in protein abundance was compared between white and dark hairs. The gene list (Supplemental Table S1) used for downstream analyses includes downregulated (<0.8-fold, n=23) and upregulated (>1.5-fold, n=67) proteins.

Experiment 2: 1 cm hair samples from each subject (n=17) were washed in 1 ml of 20% methanol while agitating at 1400 rpm for 20 mins at room temperature. The washed hair samples were homogenized using 150 µL of lysis buffer (4% SDS/0.1M Tris/Protease inhibitor

cocktail) in a glass homogenizer until no hair particles are visible. The lysates were incubated at 65°C for 13 hours overnight at 1500 rpm. The next day, the samples were centrifuged at 20,000 x g for 10 mins to clear the lysate. Cleared lysates were reduced with 5 mM DTT at room temperature for 30 mins at 1000 rpm. Alkylation was carried out with 11 mM IAA at room temperature in the dark for 30 mins and quenched with 5 mM DTT for 15 mins at room temperature. The proteins were precipitated using a chloroform-methanol method, and precipitated protein pellets were dissolved in 15 µL of resuspension buffer (4M Urea/0.1M Tris) and sonicated until entirely homogenized. Protein concentration was estimated using the BCA assay. 4 µg of total proteins from each sample was digested for 4 hours at 37°C with Lys-C protease at a 50:1 protein-to-protease ratio while shaking. Samples were then diluted with 100 mM Tris to bring down the urea concentration to the final 1.6 M and digested further with trypsin was then added at a 100:1 protein-to protease ratio, and the reaction was incubated overnight at 37°C. The next day, digestion was stopped by the addition of 1% TFA (final v/v) and centrifuged at 14,000 g for 10 min at room temperature. Cleared digested peptides were desalted on SDB-RP Stage-Tip and dried in a speed-vac. Peptides were dissolved in 3% acetonitrile/0.1% formic acid and 200 ng of peptides were injected on an Orbitrap Fusion Tribrid mass spectrometer (Thermo Scientific) coupled to an UltiMate 3000 UHPLC (Thermo Scientific). Peptides were separated on a 25 cm column (i.d. 75 µm, EASY-Spray, 2 µm, 100 Å) using a non-linear gradient of 5%-35% at a flow rate of 300 nl/min using a buffer B (0.1% (v/v) formic acid, 100% acetonitrile) for 90 min. After each gradient, the column was washed with 90 % buffer B for 5 min and re-equilibrated with 98% buffer A (0.1% formic acid, 100% HPLC-grade water) for 15 min. The full MS spectra were acquired in the Orbitrap from 400 to 1500 *m/z* at 120K with a 2 x 10^5 ion count target and a maximum injection time of 50 ms. The instrument was set to run in top speed mode with 3-second cycles for the survey and the MS/MS scans. After a survey scan, MS/MS was performed on the most abundant precursors, i.e., those exhibiting a charge state from 2 to 6 of greater than 5 x 10^3 intensity, by isolating them in the quadrupole at 1.6 Th. We used collision-induced dissociation (CID) with 35% collision energy and detected the resulting fragments with the rapid scan rate in the ion trap. The automatic gain control (AGC) target for MS/MS was set to 1 x 10^4, and the maximum injection time was limited to 35 ms. The dynamic exclusion was set to 30 s with a 10-ppm mass tolerance around the precursor and its isotopes. Monoisotopic precursor selection was enabled.

Raw mass spectrometric data were analyzed using the MaxQuant environment v.1.6.1.0[56] and Andromeda[57] for database searches at default settings with a few modifications. The default is used for first search tolerance and main search tolerance (20 ppm and 6 ppm,

respectively). MaxQuant was set up to search with the reference human UniProtKB proteome database downloaded from UniProt. MaxQuant performed the search trypsin digestion with up to 2 missed cleavages. Peptide, site, and protein false discovery rates (FDR) were all set to 1% with a minimum of 1 peptide needed for identification; label-free quantitation (LFQ) was performed with a minimum ratio count of 1. Search criteria included carbamidomethylation of cysteine as a fixed modification, oxidation of methionine, acetyl (protein N-terminus) and deamination for asparagine or glutamine (NQ) as variable modifications. A total of 438 proteins were detected. Proteins not detected in at least three samples from a total of 11 were not included in downstream analyses. Detected proteins not mapped to known genes are labeled as 'unknown'. From the eligible proteins (n=192), the fold change in protein abundance was compared between white and dark hairs. The gene list (Supplemental Table S2) used for downstream analyses includes downregulated (<0.8-fold, n=56) and upregulated (>1.5-fold, n=106) proteins. In sensitivity analyses, the data was re-analyzed with an alternate criterion of detection in at least 2 samples per color (≥2/6 dark, ≥2/5 white) and the data presented in **Supplemental Figure S10**.

For both Experiment 1 and 2, functional enrichment analysis was performed at an FDR threshold of 0.05 using Gene Ontology (GO) and Kyoto Encyclopedia of Genes and Genomes (KEGG) annotations in ShinyGO v.0.61 (http://bioinformatics.sdstate.edu/go/)[58]. Protein-protein interaction (PPI) networks were generated, analyzed for network metrics, and visualized in STRING v.11.0 (https://string-db.org/cgi/input.pl)[59]. Given the substantial representation of mitochondrial proteins among upregulated lists (67 of 323, 26.8% in Experiment 1; 21 of 106, 19.8% in white vs dark Experiment 2), we queried MitoCarta 2.0[21] and other sources, including GeneCards.org and database annotations to identify the following proteins as mitochondrial: HSP90B1, ASS1, MT-CO2[60], RPS3[61], RACK1[62], and ACOT7[63]. This search revealed enrichment of proteins related to energy metabolism and known to localize in mitochondria particularly among upregulated genes. We also queried the Human Lysosome Gene Database (http://lysosome.unipg.it/) to identify lysosomal proteins. In ShinyGO, networks of GO biological processes generated using a P-value cutoff for FDR of 0.01, and displaying top 20 most significant terms, with an edge cutoff of 0.2 were also examined to inform the functional categories that most accurately define both down- and upregulated proteins. PPI and GO biological processes networks are shown in Supplemental Figures S2-3.

Retrospective assessments of life events and stress

A subset of participants with noteworthy patterns of single-hair graying and reversal were asked to complete a retrospective stress assessment (**Supplemental Figure S6**), completed 1-4 months after hair collection in two individuals (one male, one female). In the retrospective assessment, participants are first asked to identify the most stressful event or period over the last 12 months and to position it in time along the physical timeline, using their electronic calendar and objective dates, and assign it "10" on the graph. Participants then identified the least stressful event or period and assigned it "0" on the physical timeline. Participants then indicated 2-6 additional particularly stressful events or periods, marked them on the timeline, and connected these events with a line that best illustrates their stress levels over the past year. Stress graphs were then digitized by aligning the retrospective assessment to a grid printed on transparency film, and the resulting digital values were plotted (Prism 8). To align stress profiles with HPP, digitized stress profiles were aligned with hairs from the same participant using dates of collection and assuming a hair growth rate of 1cm/month[16]. Each hair segment can then be mapped to specific weeks or month along the stress profile.

Hair shaft mtDNA quantification

Dark and white hairs (n=10 per person per color) were collected from the same two individuals whose hairs were analyzed by electron microscopy (African American male, Caucasian male). The bulb and proximal portion (2cm segment) of the hair shaft were sectioned and separately lysed in 200ul of lysis buffer containing 500 mM Tris, 1% Tween 20, 20 µg/µl Proteinase K incubated for 10 hours at 55°C, followed by 10 min at 95°C as described previously[64]. Hair bulbs were fully digested whereas the more robust proteinaceous hair shafts were only partially digested, such that the quantified DNA abundance is likely an underestimation of the total DNA amount per unit of hair shaft.

The number of mtDNA copies per nucleated cell (mtDNA copy number, mtDNAcn) was measured by real-time quantitative polymerase chain reaction (qPCR) using a duplex Taqman reaction to amplify both mitochondrial (ND1) and nuclear DNA (B2M, single-copy gene) amplicons. The primer sequences are: (ND1-Fwd: GAGCGATGGTGAGAGCTAAGGT, ND1-Rev: CCCTAAAACCCGCCACATCT, Probe: HEX-CCATCACCCTCTACATCACCGCCC-3IABkFQ. B2M-Fwd: CCAGCAGAGAATGGAAAGTCAA, B2M-Rev: TCTCTCTCCATTCTTCAGTAAGTCAACT, Probe:FAMATGTGTCTGGGTTTCATCCATCCGACA-3IABkFQ) obtained from IDTdna.com. qPCR was performed on *QuantStudio™ 7 Flex Real-Time PCR System* (Applied Biosystems, Foster City, CA). Cycling conditions were as follows; 1 cycle of 50°C for 2 min, 95°C for 20 sec, followed by 40 cycles of 95°C for 1 sec, 60°C 20 sec.

25

For bulbs, all ND1 and B2M Cts were in the dynamic range of the assay and used to compute mtDNAcn from the ΔCt. All measures were performed in triplicates and the average Ct values taken for each sample. The mean C.V. for ND1 was 0.67% in both shafts and bulbs, and for B2M 0.52% in bulbs. mtDNAcn was calculated as $2^{\Delta Ct}$ (ND1 Ct - B2M Ct), and multiplied by 2 to take into account the diploid nature of the nuclear genome. In hair shafts, the average B2M Ct value was 35.2 Cts, and therefore considered uninterpretable or undetectable, so only ND1 data was analyzed for shafts.

Mathematical modeling of graying dynamics across the lifespan

To simulate hair graying across the lifespan, a linear mixed effect model with random intercept and slopes to account for the stochastic process of hair graying was implemented in R[65]. This interactive implementation is available at https://timrain.shinyapps.io/hair. We first hypothesized a potential mechanism in which individual hairs are affected by a summation of effects from a random aging factor accumulating over time, random stress factor and random initial graying loading, thus creating variation between hairs within an individual. Once the hair has passed a prespecified threshold, the hair transitions to gray (**Figure 5B**). This model includes 17 parameters listed in **Supplemental Table S4**, each of which can be adjusted to simulate various effects on individual hairs in relation to the aging process, including one or two stress exposure periods with customizable intensity and duration.

Scaling this model to hair populations with thousands of hairs, the simulation reports trajectories of graying for individual hairs, as well as a graph with the population distribution of white hairs (shown as frequency distributions) for a theoretical scalp. First, we simulated the average graying trajectory based on data indicating that the average age of onset for graying is age 35 and that white hairs reach a 40% population frequency at age 65[6]. This established a set of default parameters that yielded the graying trajectory shown in Figure 5C. We then simulated two hypothetical scenarios reflecting the total hair population for individuals who accumulate gray hairs at different rates, termed early and late grayers. These variable graying patterns were found to be generated by changing only one parameter, Sigma1, the standard deviation (across HFs) of the rate at which the aging factor increases over time.

Additionally, the model also simulated graying reversal, beginning with the parameters of the average grayer and then including also the stress parameters. To show the effect of stress on hair graying, we simulated two stressful periods starting at age 20 and then again at age 50, with equal intensity and duration. At age 20 the aging factor increases due to the stress but

26

does not induce gray hair as the aging factor is still below the threshold (Figure 5E). On the other hand, at age 50 the same intensity and duration of the stressor will tend to induce additional graying as the aging factor for some hairs increases past the threshold, and then upon the end of the stressor, the aging factor could decreases past the threshold and thus the hair would undergo reversal (i.e., repigmentation) to its original color (Figure 5F).

An alternative model was considered to explore potential mechanisms for hair transitioning and reversal in response to stress. Specifically, we considered a mechanism in which the *rate* of accumulation in the aging factor increases during a period of stress (as opposed to our final model where stress causes a stepwise increase in aging factor) and then returns to the original rate following the end of the stressor. In this scenario, the threshold remains constant. This mechanism can be rejected because although it adequately simulates hair graying, once a hair has crossed above the threshold, if the stressor only affects the slope, it is not possible for a hair to return below threshold and undergo reversal (**Supplemental Figure S11**).

To simulate the graying process for a hypothetical person based on our hypothesized mechanism, we posited a linear mixed model for the ith ($i = 1, ..., n$) hair with two fixed effects (β_1 aging factor rate and β_2 stress sensitive rate) and three random effects (b_{i0} for graying loading at age 0, b_{i1} for aging factor rate and b_{i2} for stress sensitive rate). To ensure positivity in age and accumulating stress, the model involves only the absolute value of each random effect.

$$Graying\,Loading_{\{i,age\}} = |b_{i0}| + (|b_{i1}| + \beta_1)age + (|b_{i2}| + \beta_2)Accumulating\,Stress_{\{age\}} + e_{\{i,age\}}$$

Where $Accumulating\,Stress$ is defined as:

$$Accumulating\,Stress_{age} = \sum_{a=age-WindowWidth}^{age} stress_a$$

The three random effects follow a multivariate normal:

$$(b_{i0}, b_{i1}, b_{i2}) \sim N(0, G)$$

with covariance structure:

$$G = \begin{bmatrix} \sigma_0^2 & \rho_{01}\sigma_0\sigma_1 & \rho_{02}\sigma_0\sigma_2 \\ \rho_{01}\sigma_1\sigma_0 & \sigma_1^2 & \rho_{12}\sigma_1\sigma_2 \\ \rho_{02}\sigma_2\sigma_0 & \rho_{12}\sigma_2\sigma_1 & \sigma_2^2 \end{bmatrix}$$

All the correlations $\rho_{01}, \rho_{02}, \rho_{12}$ in the simulation are constrained to be positive. When the aging factor of hair i reaches a predefined threshold, the ith hair will turn white. The source code is available at https://github.com/junting-ren/hair_simulation.

Statistical analyses

An ordinary one-way ANOVA with Tukey's multiple comparison test was used to compare the number of Granules per μm^2, granule size, granule intensity, and relative intensity of the cortex in the dark and white hairs, and to compare the pigmentation intensity across head regions. To compare the rate of change in pigmentation per day between graying and reversal hairs, points of transitions visually estimated were used to derive a slope for each graying or reversal segment, which were compared using an unpaired t test.

A Mann-Whitney test was used to compare mtDNA levels in dark and white hair shafts and mtDNA copy number in dark and white hair bulbs.

For univariate and multivariate analyses of proteomic signatures, protein abundance levels were processed in R using the Metaboanalyst 3.0 platform[66] as unpaired data. The data was mean-centering and log transformed prior to statistical analyses and missing (low abundance) values were imputed by half of the lowest value for the group (dark, white). Significance was established at an FDR level 0.05 and fold changes calculated using ANOVA. Partial least square discriminant analysis (PLS-DA) was used to extract meaningful features that distinguish dark and white hairs and visualize groups of hairs or segments along the same hair. Two different strategies were used to generate protein lists subsequently queried for their functional significance: i) For dark vs white comparisons where the whole model is meaningful, the variable importance in projection (VIP) scores for each protein were extracted and used to select the top 40 most influential proteins (**Supplemental Figure S4C**); ii) For analyses of segments along the hair with graying followed by reversal, the factor loadings for each protein were extracted separately for components 1 and 2, and the top 20 positive and 20 negative proteins were selected for further analysis. Protein lists derived from both strategies were then used for functional enrichment analysis in ShinyGO and STRING as described above.

For the data displayed in Figure 3, we measured the strength of the temporal relationship between time series on the same scale (e.g., intensity measures of two hairs) by calculating the mean squared differences. The overall strength of temporal relationship among multiple time series is measured by the sum of all pairwise mean squared differences. To measure the strength of the temporal relationship between time series on different scales (specifically, intensity of color for a hair and rated level for stress levels) we calculated Pearson's correlation. To provide a reference distribution for comparison, we conducted 1000

random permutations of the data in each instance. For Figures 3A and 3B, each permutation involved simulating an equivalent number of hairs that transition (three graying hairs in 3A; two reverting hairs in 3B). Each simulated hair includes a randomly selected transition placed at a random time point, with resampled noise before and after the transition. The library of transitions was taken from the transition segments of each observed hair that underwent the same directional change (dark-to-white in 3A; white-to-dark in 3B). The noise for uses of resampling was taken from hairs from the same subject after subtracting a smooth function, and resampling was done in segments of length-100 increments to maintain proper temporal correlation patterns. For Figure 3D, under the null hypothesis of no relationship between the hair intensity and stress pattern, each permutation involved choosing a random time point, splitting the stress pattern at that point and rejoining it by concatenating the two segments in the alternative order.

Additional References:

55   Picard, M., White, K. & Turnbull, D. M. Mitochondrial morphology, topology, and membrane interactions in skeletal muscle: a quantitative three-dimensional electron microscopy study. *J Appl Physiol (1985)* **114**, 161-171, doi:10.1152/japplphysiol.01096.2012 (2013).

56   Cox, J. & Mann, M. MaxQuant enables high peptide identification rates, individualized p.p.b.-range mass accuracies and proteome-wide protein quantification. *Nat Biotechnol* **26**, 1367-1372, doi:10.1038/nbt.1511 (2008).

57   Cox, J. *et al.* Andromeda: a peptide search engine integrated into the MaxQuant environment. *J Proteome Res* **10**, 1794-1805, doi:10.1021/pr101065j (2011).

58   Ge, S. X., Jung, D. & Yao, R. ShinyGO: a graphical enrichment tool for animals and plants. *Bioinformatics*, doi:10.1093/bioinformatics/btz931 (2019).

59   Szklarczyk, D. *et al.* STRING v11: protein-protein association networks with increased coverage, supporting functional discovery in genome-wide experimental datasets. *Nucleic Acids Res* **47**, D607-D613, doi:10.1093/nar/gky1131 (2019).

60   Gustafsson, C. M., Falkenberg, M. & Larsson, N. G. Maintenance and Expression of Mammalian Mitochondrial DNA. *Annu Rev Biochem* **85**, 133-160, doi:10.1146/annurev-biochem-060815-014402 (2016).

61   Kim, Y., Kim, H. D. & Kim, J. Cytoplasmic ribosomal protein S3 (rpS3) plays a pivotal role in mitochondrial DNA damage surveillance. *Biochim Biophys Acta* **1833**, 2943-2952, doi:10.1016/j.bbamcr.2013.07.015 (2013).

62   Lin, W. *et al.* The association of receptor of activated protein kinase C 1(RACK1) with infectious bursal disease virus viral protein VP5 and voltage-dependent anion channel 2 (VDAC2) inhibits apoptosis and enhances viral replication. *J Biol Chem* **290**, 8500-8510, doi:10.1074/jbc.M114.585687 (2015).

63   Bekeova, C. *et al.* Multiple mitochondrial thioesterases have distinct tissue and substrate specificity and CoA regulation, suggesting unique functional roles. *J Biol Chem* **294**, 19034-19047, doi:10.1074/jbc.RA119.010901 (2019).

64   Picard, M. *et al.* Mitochondrial dysfunction and lipid accumulation in the human diaphragm during mechanical ventilation. *Am J Respir Crit Care Med* **186**, 1140-1149, doi:10.1164/rccm.201206-0982OC (2012).

65   R: A language and environment for statistical computing. (R Foundation for Statistical Computing, Vienna, Austria, 2010).

66   Chong, J., Wishart, D. S. & Xia, J. Using MetaboAnalyst 4.0 for Comprehensive and Integrative Metabolomics Data Analysis. *Curr Protoc Bioinformatics* **68**, e86, doi:10.1002/cpbi.86 (2019).

Acknowledgements

Author contributions

A.R., S.R., R.K.S., P.T., G.S.: collected data. AR, SR, CL, RTO, MP: analyzed data. JR, RTO: developed the simulation model with SR. AR, EM: performed imaging. MP, RP: drafted manuscript. MP, GS: designed study. All authors contributed to data interpretation and the final version of the manuscript.

Supplementary Information is available for this paper

The supplemental material includes 12 Figures (Figures S1-S12), 4 Tables (Tables S1-S4), and 1 Video (Video S1).

Correspondence and requests for materials should be addressed to Martin Picard, martin.picard@columbia.edu

Figure legends

Figure 1. Quantitative analysis of human hair pigmentation patterns, graying, and associated proteomic changes. (**A**) Diagram illustrating hair growth over time, method of hair collection, digitization, and hair pigmentation pattern (HPP) methodology. (**B**) Dark, white, and hairs undergoing natural age-related transitions from the younger dark state to the older white state at macroscopic and microscopic resolution. (**C**) Digitized HPPs for the hairs shown in (B). (**D**) Bright field microscopy images of hair bulbs from plucked dark (top-panel) and white hair (bottom-panel) from the same Caucasian male individual illustrating the loss of pigmentation in the hair follicle pigmentary unit (HFPU). (**E**) Electron microscopic images of dark (*top*) and white (*bottom*) scalp hairs from a Caucasian male showing absent melanin granules in white hairs. (**F**) Quantification from dark (D) and white (W) hairs from a Caucasian (Cau.) male and African American (AA) male of melanin granule abundance, (**G**) size and (**H**) darkness. (**I**) Overall electron density of the hair matrix (excluding granules) (N.S.). **J**) Volcano plot comparing dark and white hair proteomes and (**K**) heatmap of down- (<0.8-fold) and up-regulated (>1.5-fold) proteins that were detected in all samples for experiment 1 (duplicates of dark/white hairs from 1 female, 1 male, n=8 samples). (**L**) Volcano plot and (**M**) heatmap for all proteins from experiment 2 (dark and white hairs from 6 individuals, n=6 dark and 5 white hairs). Proteins annotated as mitochondrial (Mitocarta2.0) and lysosomal (The Human Lysosome Gene Database) are highlighted. Red dots to the right of heatmaps indicate mitochondrial proteins. *P<0.05, **P<0.01, ****P<0.0001 from one-way ANOVA, Tukey's multiple comparisons.

Figure 2 – Reversal of hair graying across ages and body regions. (**A-G**) Examples of HS graying and reversal including schematic of hair growth (*top left*), digitized HPP (*top right*), and light microscopy images (*bottom*) corresponding to numbered HS segments on the HPP plot. (**A**) Examples illustrating the reversal of graying along the length of scalp, (**B**) pubic, (**C**) and beard human HSs. (**D**) Example of segmental HS with double transitions, including temporary graying and (**E**) temporary reversal from an adult and a child, respectively. See Supplemental Figure S5 for additional examples and Video S1 for animation. (**F**) Time course diagram illustrating the progression of a single dark HS undergoing graying followed by reversal back to its original color, and (**G**) closely occurring events of graying and reversal occurring, producing HS with double transitions. (**H**) Average maximum and minimum pigmentation intensity among transitioning hairs from participants with two-colored hairs (n=11). Hairs with an average maximum intensity >180 A.U. are categorized as high intensity (black), 140-180 A.U. as intermediate intensity, and 100-140 A.U. as low intensity (pale color), indicating that these findings generalize across a range of pigmentation densities. (**I**) Rate of depigmentation per day in graying HS, measured from the slope on HPP graphs expressed as % of starting intensity loss per day (assuming growth rate of 1cm/month). (**J**) Comparison of the absolute rate of pigmentation change per day in graying and reverted HS. I and J are reported on a $\log_2$ scale to facilitate visualization.

Figure 3 – Synchronous graying and reversal behavior across multiple hairs and associations with psychosocial stress. (**A**) In a 35-year old Caucasian female, multiple HS (n=3) undergoing graying simultaneously. (**B**) In a 37-year old Caucasian female, two bi-color HS collected two months apart aligned based on a growth rate of 1cm/month undergoing reversal nearly simultaneously. In A and B, simultaneously plucked dark and white hairs are plotted for reference. (**C**) In a 35-year old Caucasian male, multiple bi-color HS (n=5) undergoing reversal (top-panel) plotted against time-matched self-reported psychosocial stress levels (bottom-panel). (**D**) HS from a 30- year old Asian female with two months of self-reported profound perceived stress associated with temporary hair graying and reversal. Note the synchronicity between the increase in stress and rapid depigmentation (i.e., graying), followed by complete (103%) recovery of HS pigmentation (i.e., reversal of graying) upon alleviation of life stress. (**E**) Heatmap of protein abundance (n=301) across 6 segments: 2 dark prior to stress/graying, 2 white following graying, 2 dark segments after reversal. (**F**) Multivariate PLS-DA model of the 6 segments from the HS in E, highlighting the model's first and second principal components related to graying and reversal, respectively. Numbers 1 to 6 correspond to HS segments on D. (**G**) Factor loadings for Components 1 and 2 were used to extract the most significant proteins, subsequently analyzed for functional enrichment categories in KEGG and GO databases, and STRING protein networks. (**H**) Trajectories of protein abundance from the top Component 1 and (**I**) Component 2 features across the 6 segments; proteins with positive (*top*) and negative loadings (*bottom*) are shown separately.

Figure 4 – Meta-analysis of human hair proteomic findings comparing dark and white hairs. (**A**) Number of downregulated (<0.8-fold, blue) and upregulated (<1.5-fold) proteins across datasets, and unchanged proteins shown in grey. (**B**) Venn diagram illustrating the intersection of datasets. The number of overlapping proteins across datasets that are either consistently down- or upregulated, or proteins not regulated in the same direction, are shown for each area of overlap. (**C**) Individual protein abundance for consistently upregulated (n=5) and downregulated proteins (n=2) across experiments 1 and 2 shown as violin plots with median. (**D**) Mitochondrial DNA abundance in human HS of the same two donors as in Figures 1F-I (AA male, Cau male). (**E**) Summary of significantly enriched KEGG categories across datasets, for upregulated (*left*) and downregulated (*right*) proteins. (**F**) Correlation matrix (Spearman's r) of all detected proteins (n=192) in experiment 2, illustrating general human hair protein co-expression across dark and white pigmented states (dark, white). Four main clusters are highlighted and labeled by their top KEGG category. N.S. from Mann Whitney Test.

Figure 5 – Modeling of hair graying and reversal across the human lifespan and in response to temporary stress. (**A**) Schematic overview of the average graying process across the lifespan involving the gradual loss of pigmentation, or accumulation of white hairs, mostly in the second two-thirds of life. (**B**) Depiction of individual hairs (each line is a hair, i) from a linear mixed effects model with random intercept and slopes predicting hair graying. The model assumes i) a constant increase in a putative aging factor and ii) a constant threshold above which hairs undergo depigmentation. All model

parameters are listed in Supplemental Table S4. (**C**) Predicted hair population behavior (n=1,000 hairs) shown as a cumulative frequency distribution of white hairs from the individual trajectories in panel (B). (**D**) Frequency distributions of gray hairs for individuals with early (*left)*, average (*middle*), or late (*right*) hair graying phenotypes. The inset highlights a 2-year period during mid-life indicating gradual accumulation of white hairs, as well as the spontaneous repigmentation of a small fraction of white hairs (decrease in % white hairs), consistent with real-world data. (**E**) Single hair-level and (**F**) hair population-level results from the addition of two acute stress periods (each one year in duration, occurring at ages 20 and 50). The optimized model accounts for stress-induced graying in hairs whose aging factor is close to the depigmentation threshold, but not for young hairs or those far away from the threshold. Similarly, the removal of the stressor causes repigmentation of hairs when the aging factor returns below the threshold.
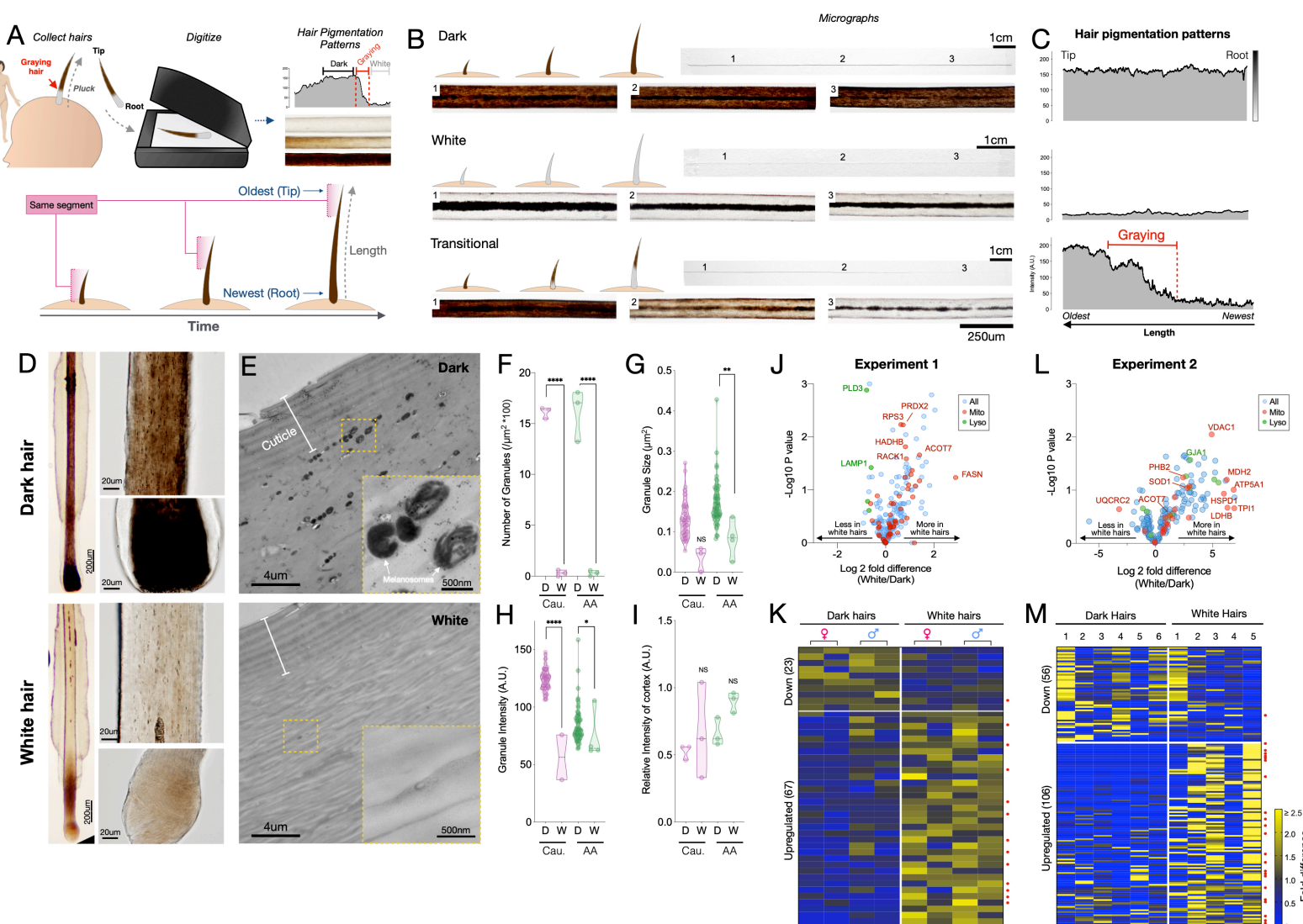
Figure 1. Quantitative analysis of human hair pigmentation patterns, graying, and associated proteomic changes. (**A**) Diagram illustrating hair growth over time, method of hair collection, digitization, and hair pigmentation pattern (HPP) methodology. (**B**) Dark, white, and hairs undergoing natural age-related transitions from the younger dark state to the older white state at macroscopic and microscopic resolution. (**C**) Digitized HPPs for the hairs shown in (B). (**D**) Bright field microscopy images of hair bulbs from plucked dark (top-panel) and white hair (bottom-panel) from the same Caucasian male individual illustrating the loss of pigmentation in the hair follicle pigmentary unit (HFPU). (**E**) Electron microscopic images of dark (*top*) and white (*bottom*) scalp hairs from a Caucasian male showing absent melanin granules in white hairs. (**F**) Quantification from dark (D) and white (W) hairs from a Caucasian (Cau.) male and African American (AA) male of melanin granule abundance, (**G**) size and (**H**) darkness. (**I**) Overall electron density of the hair matrix (excluding granules) (N.S.). **J**) Volcano plot comparing dark and white hair proteomes and (**K**) heatmap of down- (<0.8-fold) and up-regulated (>1.5-fold) proteins that were detected in all samples for experiment 1 (duplicates of dark/white hairs from 1 female, 1 male, n=8 samples). (**L**) Volcano plot and (**M**) heatmap for all proteins from experiment 2 (dark and white hairs from 6 individuals, n=6 dark and 5 white hairs). Proteins annotated as mitochondrial (Mitocarta2.0) and lysosomal (The Human Lysosome Gene Database) are highlighted. Red dots to the right of heatmaps indicate mitochondrial proteins. *P<0.05, **P<0.01, ****P<0.0001 from one-way ANOVA, Tukey's multiple comparisons.
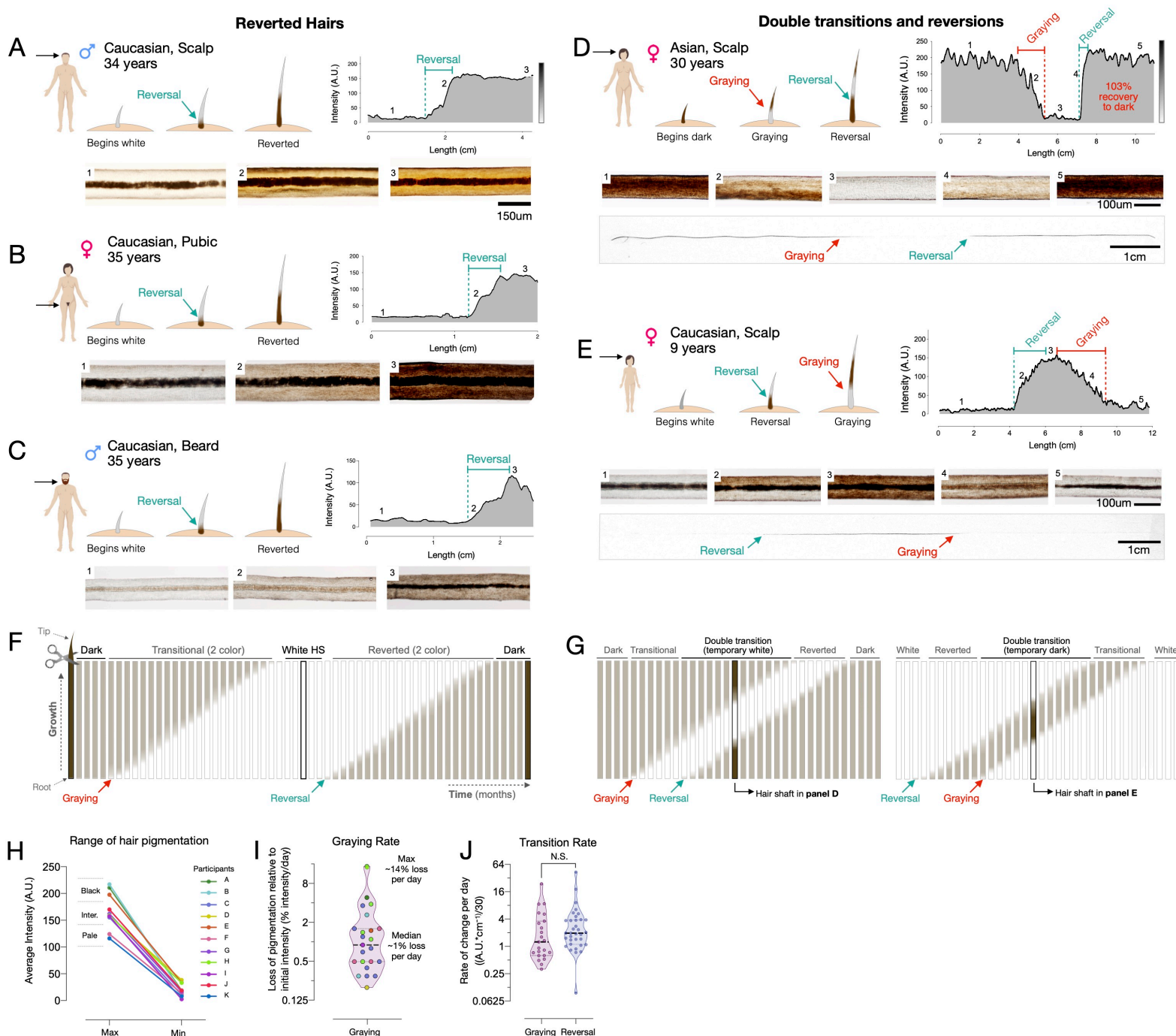
Figure 2 – Reversal of hair graying across ages and body regions. (**A-G**) Examples of HS graying and reversal including schematic of hair growth (*top left*), digitized HPP (*top right*), and light microscopy images (*bottom*) corresponding to numbered HS segments on the HPP plot. (**A**) Examples illustrating the reversal of graying along the length of scalp, (**B**) pubic, (**C**) and beard human HSs. (**D**) Example of segmental HS with double transitions, including temporary graying and (**E**) temporary reversal from an adult and a child, respectively. See Supplemental Figure S5 for additional examples and Video S1 for animation. (**F**) Time course diagram illustrating the progression of a single dark HS undergoing graying followed by reversal back to its original color, and (**G**) closely occurring events of graying and reversal occurring, producing HS with double transitions. (**H**) Average maximum and minimum pigmentation intensity among transitioning hairs from participants with two-colored hairs (n=11). Hairs with an average maximum intensity >180 A.U. are categorized as high intensity (black), 140-180 A.U. as intermediate intensity, and 100-140 A.U. as low intensity (pale color), indicating that these findings generalize across a range of pigmentation densities. (**I**) Rate of depigmentation per day in graying HS, measured from the slope on HPP graphs expressed as % of starting intensity loss per day (assuming growth rate of 1cm/month). (**J**) Comparison of the absolute rate of pigmentation change per day in graying and reverted HS. I and J are reported on a log$_2$ scale to facilitate visualization.
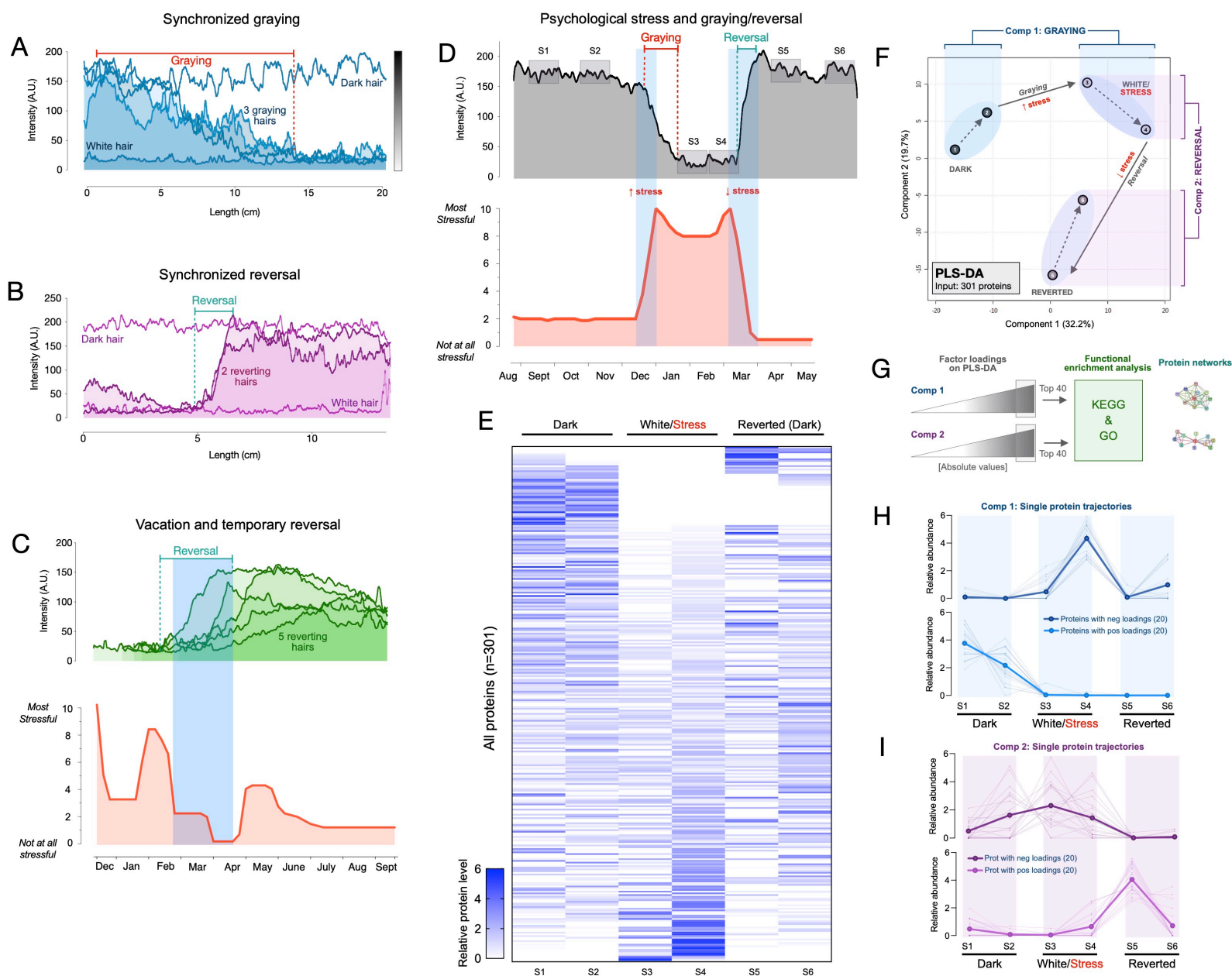
Figure 3 – Synchronous graying and reversal behavior across multiple hairs and associations with psychosocial stress. (A) In a 35-year old Caucasian female, multiple HS (n=3) undergoing graying simultaneously. **(B)** In a 37-year old Caucasian female, two bi-color HS collected two months apart aligned based on a growth rate of 1cm/month undergoing reversal nearly simultaneously. In A and B, simultaneously plucked dark and white hairs are plotted for reference. **(C)** In a 35-year old Caucasian male, multiple bi-color HS (n=5) undergoing reversal (top-panel) plotted against time-matched self-reported psychosocial stress levels (bottom-panel). **(D)** HS from a 30- year old Asian female with two months of self-reported profound perceived stress associated with temporary hair graying and reversal. Note the synchronicity between the increase in stress and rapid depigmentation (i.e., graying), followed by complete (103%) recovery of HS pigmentation (i.e., reversal of graying) upon alleviation of life stress. **(E)** Heatmap of protein abundance (n=301) across 6 segments: 2 dark prior to stress/graying, 2 white following graying, 2 dark segments after reversal. **(F)** Multivariate PLS-DA model of the 6 segments from the HS in E, highlighting the model's first and second principal components related to graying and reversal, respectively. Numbers 1 to 6 correspond to HS segments on D. **(G)** Factor loadings for Components 1 and 2 were used to extract the most significant proteins, subsequently analyzed for functional enrichment categories in KEGG and GO databases, and STRING protein networks. **(H)** Trajectories of protein abundance from the top Component 1 and **(I)** Component 2 features across the 6 segments; proteins with positive (*top*) and negative loadings (*bottom*) are shown separately.
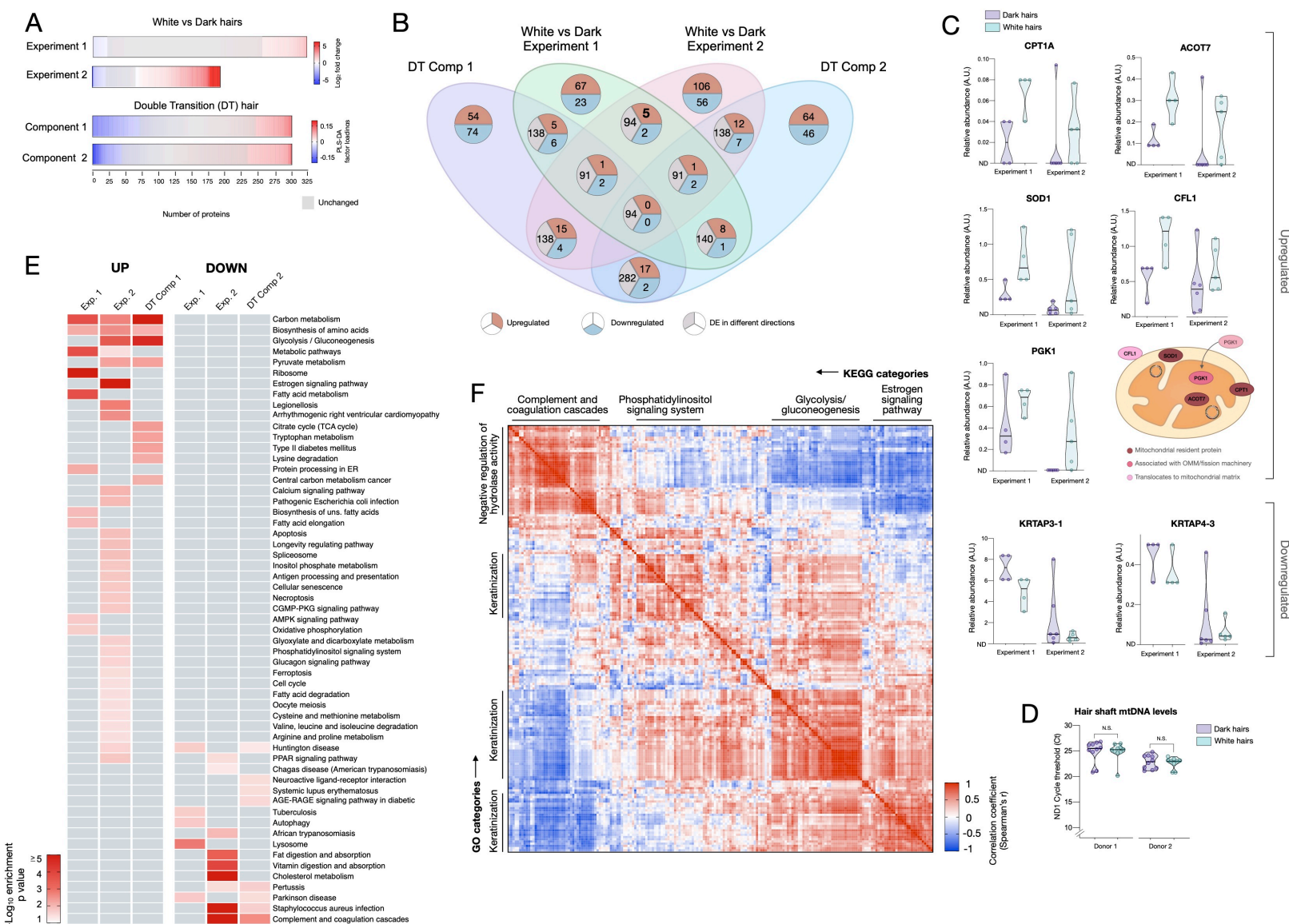
Figure 4 – Meta-analysis of human hair proteomic findings comparing dark and white hairs. (**A**) Number of downregulated (<0.8-fold, blue) and upregulated (<1.5-fold) proteins across datasets, and unchanged proteins shown in grey. (**B**) Venn diagram illustrating the intersection of datasets. The number of overlapping proteins across datasets that are either consistently down- or upregulated, or proteins not regulated in the same direction, are shown for each area of overlap. (**C**) Individual protein abundance for consistently upregulated (n=5) and downregulated proteins (n=2) across experiments 1 and 2 shown as violin plots with median. (**D**) Mitochondrial DNA abundance in human HS of the same two donors as in Figures 1F-I (AA male, Cau male). (**E**) Summary of significantly enriched KEGG categories across datasets, for upregulated (*left*) and downregulated (*right*) proteins. (**F**) Correlation matrix (Spearman's r) of all detected proteins (n=192) in experiment 2, illustrating general human hair protein co-expression across dark and white pigmented states (dark, white). Four main clusters are highlighted and labeled by their top KEGG category. N.S. from Mann Whitney Test.
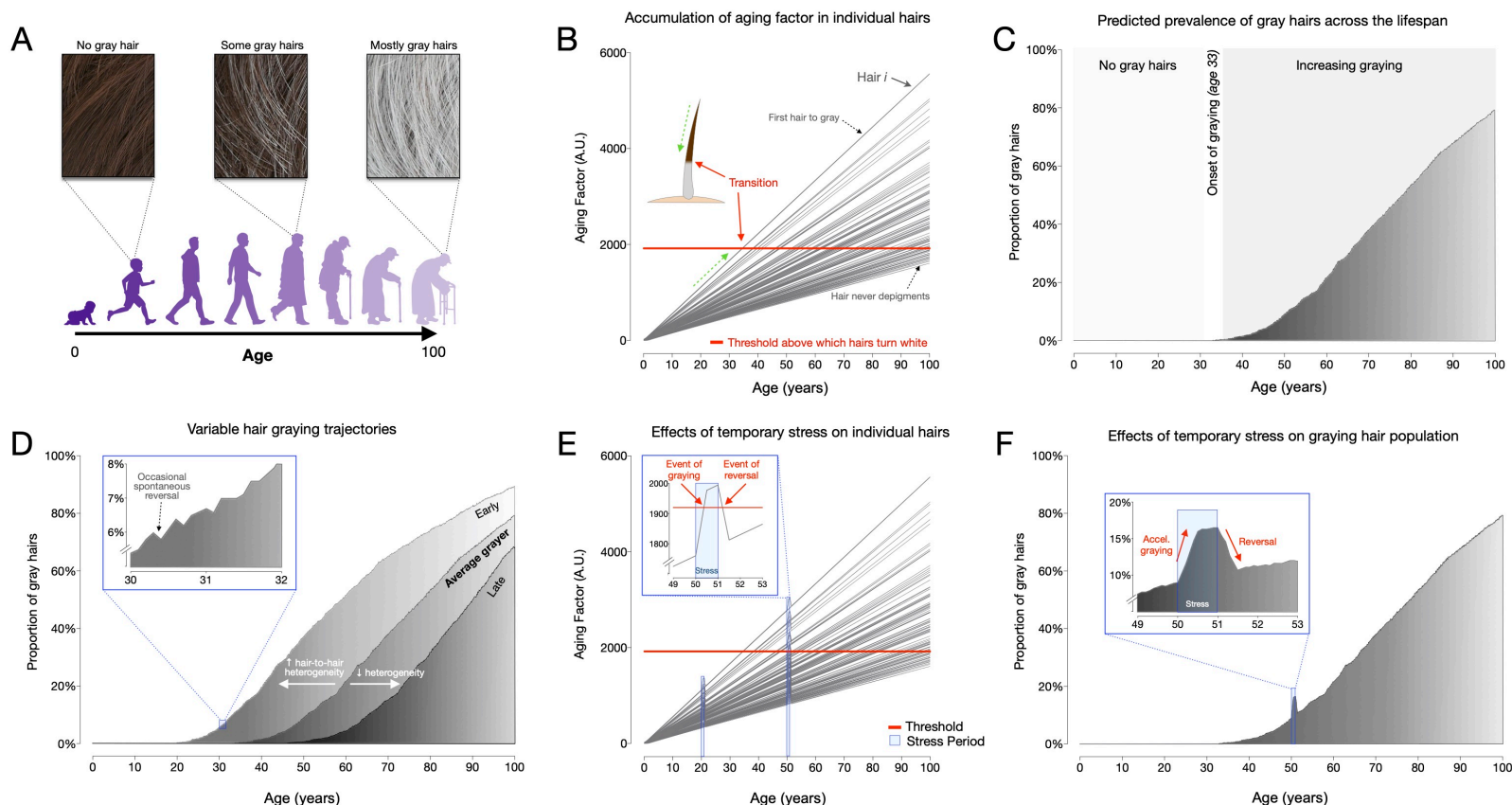
Figure 5 – Modeling of hair graying and reversal across the human lifespan and in response to temporary stress. (**A**) Schematic overview of the average graying process across the lifespan involving the gradual loss of pigmentation, or accumulation of white hairs, mostly in the second two-thirds of life. (**B**) Depiction of individual hairs (each line is a hair, i) from a linear mixed effects model with random intercept and slopes predicting hair graying. The model assumes i) a constant increase in a putative aging factor and ii) a constant threshold above which hairs undergo depigmentation. All model parameters are listed in Supplemental Table S4. (**C**) Predicted hair population behavior (n=1,000 hairs) shown as a cumulative frequency distribution of white hairs from the individual trajectories in panel (B). (**D**) Frequency distributions of gray hairs for individuals with early (*left*), average (*middle*), or late (*right*) hair graying phenotypes. The inset highlights a 2-year period during mid-life indicating gradual accumulation of white hairs, as well as the spontaneous repigmentation of a small fraction of white hairs (decrease in % white hairs), consistent with real-world data. (**E**) Single hair-level and (**F**) hair population-level results from the addition of two acute stress periods (each one year in duration, occurring at ages 20 and 50). The optimized model accounts for stress-induced graying in hairs whose aging factor is close to the depigmentation threshold, but not for young hairs or those far away from the threshold. Similarly, the removal of the stressor causes repigmentation of hairs when the aging factor returns below the threshold.